AIP | The Journal of Chemical Physics

Infrared spectroscopy and modeling of co-crystalline CO2·C2H2 aerosol particles. I. The formation and decomposition of co-crystalline CO2·C2H2 aerosol particles

Thomas C. Preston, Chia C. Wang, and Ruth Signorell

Citation: The Journal of Chemical Physics **136**, 094509 (2012); doi: 10.1063/1.3690063
View online: http://dx.doi.org/10.1063/1.3690063
View Table of Contents: http://scitation.aip.org/content/aip/journal/jcp/136/9?ver=pdfcov
Published by the AIP Publishing

THE JOURNAL OF CHEMICAL PHYSICS **136**, 094509 (2012)

Infrared spectroscopy and modeling of co-crystalline $CO_2 \cdot C_2H_2$ aerosol particles. I. The formation and decomposition of co-crystalline $CO_2 \cdot C_2H_2$ aerosol particles

Thomas C. Preston, Chia C. Wang, and Ruth Signorell[a]
Department of Chemistry, University of British Columbia, 2036 Main Mall, Vancouver, British Columbia V6T 1Z1, Canada

(Received 29 September 2011; accepted 9 February 2012; published online 6 March 2012)

Aerosol particles composed of co-crystalline $CO_2 \cdot C_2H_2$ were generated in a bath gas cooling cell at cryogenic temperatures and investigated with infrared spectroscopy between 600 and 4000 cm^{-1}. Similar to results obtained for thin films of the co-crystal [T. E. Gough and T. E. Rowat, J. Chem. Phys. **109**, 6809 (1998)], this phase was found to be metastable and decomposed into pure CO_2 and pure C_2H_2. These decomposed aerosols were characterized through (i) a comparison to experimentally prepared aerosols of mixed CO_2 and C_2H_2 of known architectures and (ii) the modeling of infrared spectra. A likely architecture after decomposition are C_2H_2-CO_2 core-shell particles with a disk-like shape. The co-crystalline $CO_2 \cdot C_2H_2$ aerosols prior to decomposition are modeled and analyzed in detail in the subsequent paper (Part II). © *2012 American Institute of Physics*. [http://dx.doi.org/10.1063/1.3690063]

I. INTRODUCTION

Aerosol ice particles, such as C_2H_2, CO_2, and mixed C_2H_2/CO_2 particles play an important role in the atmospheres of a number of planets and moons.[1–6] They can directly influence the radiative balance and thus the climate by absorbing and scattering the solar radiation.[2,7] They are involved in cloud formation either as a major cloud component or as cloud condensation nuclei. Furthermore, the large surface area of aerosol particles can provide reactive sites for various chemical processes.[8] As atmospheres will contain many molecular species, multicomponent aerosols are often of particular interest.[9–11] Condensation of different compounds usually happens at various altitudes in planetary atmospheres. This leads to a wealth of possible multicomponent aerosol particle structures such as core-shell structures, inclusions, or in rare cases even the formation of particles with mixed crystalline structures.

C_2H_2 is known to form a wide range of co-crystals when paired with other small molecules.[12] As CO_2 and C_2H_2 both exhibit similar sublimation pressures over a wide range of temperatures,[13] form cubic crystalline phases (Pa3),[14,15] possess electric quadrupole moments,[16] and are linear molecules of similar dimensions, these two molecules could potentially form a co-crystal. This $CO_2 \cdot C_2H_2$ phase has indeed been observed. By condensing mixtures of the two gases onto a zinc selenide window, Gough *et al.* were able confirm the formation of the $CO_2 \cdot C_2H_2$ co-crystal using infrared (IR) spectroscopy.[17–19] This was possible due to the sensitivity of the vibrational frequencies of C_2H_2 and CO_2 to the crystalline environment in which they are found. Significant shifts in most of the IR active bands led to the identification of a mixed $CO_2 \cdot C_2H_2$ phase. However, the structure of this co-crystal was not established. A surprising observation from this work was that this $CO_2 \cdot C_2H_2$ phase was metastable and over time would decompose into domains of its pure components.[18,19] This decomposition was also studied using IR spectroscopy. The observed metastability explains why in a recent x-ray diffraction study of various C_2H_2 co-crystals presented by Kirchner *et al.* it was not possible to prepare $CO_2 \cdot C_2H_2$ co-crystals.[12] In that work, samples were annealed prior to measurements and this process likely decomposed the $CO_2 \cdot C_2H_2$ phase before it could be properly characterized.

In the current and subsequent[20] contributions (hereafter referred to as Part I and Part II, respectively) we study $CO_2 \cdot C_2H_2$ aerosols. In this work (Part I), we focus on the experimental formation and decomposition of the $CO_2 \cdot C_2H_2$ aerosols and the analysis of the spectra after decomposition. Similar to Gough *et al.* we rely on IR measurements for characterization. As we are studying aerosols not thin films, measurements are performed directly in the bath gas cooling cell where the aerosol particles are formed. These in situ measurements avoid any potential complications that might be introduced if the samples were collected on substrates. Furthermore, this setup allows us to record spectra with different architectures (core-shell and mixed) that may be of interest in planetary atmospheres. IR spectra of three different types of aerosol particles are discussed: pure CO_2 and pure C_2H_2 aerosol particles (Sec. IV A), $CO_2 \cdot C_2H_2$ aerosol particles formed by the condensation of gas mixtures of C_2H_2 and CO_2 (Sec. IV B), and mixed aerosol particles containing domains of pure C_2H_2 and pure CO_2 formed either by the decomposition of the $CO_2 \cdot C_2H_2$ co-crystal or by the sequential condensation of the two gases (Sec. IV C). Our discussion primarily focuses on the conditions that allow for the formation of $CO_2 \cdot C_2H_2$ particles and the type of domains present in the particles after the $CO_2 \cdot C_2H_2$ phase decomposes into its pure components.

---

[a] Fax: +1 604 822-2847. Electronic mail: signorell@chem.ubc.ca.

In the subsequent paper (Part II), we analyze the spectra of the $CO_2 \cdot C_2H_2$ co-crystalline phase and we examine how the $CO_2 \cdot C_2H_2$ unit cell influences the position and strength of the IR bands using density functional theory. Dielectric functions that describe $CO_2 \cdot C_2H_2$ are constructed from these parameters and incorporated into model particle shapes. This process allows for the spectra of $CO_2 \cdot C_2H_2$ particles to be modeled (and provides additional verification that co-crystals are formed). A major goal of the work in Part II is the determination of possible crystal structures for the $CO_2 \cdot C_2H_2$ phase.

II. EXPERIMENTAL

Mixed $CO_2 \cdot C_2H_2$ aerosols were generated in a low temperature bath gas cooling cell and spectroscopically characterized in situ in the aerosol phase by rapid-scan Fourier transform infrared spectroscopy between 600 and 4000 cm^{-1}. The cell had an optical path length of 16 m. The experimental setup has been described in detail in Ref. 21. Briefly, aerosol particles were formed via injection of warm sample gas mixtures (0.1%−0.3% CO_2 (99.998%) and C_2H_2 (99.6%) diluted in helium (99.999%)) into a pre-cooled bath gas (helium gas at pressures between 500–900 mbar and at a temperature of 78 K). All gases were further cleaned before use in a liquid nitrogen trap. Injection of warm sample gases into the pre-cooled bath gas leads to supersaturation, which in turn results in the formation of aerosol particles. The injection was controlled by magnetic valves, with typical injection times of 500–1000 ms. Particle sizes were roughly 50 nm and the particle number density was approximately 10^6 particles/cm^3. This low density ensures that no aggregates were formed. All infrared spectra were recorded with a spectral resolution of 0.5 cm^{-1}.

For the mixed particles, we employed two different injection schemes. Homogeneously mixed binary aerosols were formed by co-condensation of premixed CO_2 and C_2H_2 gas samples. Core-shell aerosols were generated by sequential injection of the two gases. The time delay between the two sequential injections was 500 ms. This delay was adjusted to ensure optimal coating of the core but avoid any homogeneous mixing of the two substances.

III. COMPUTATIONAL METHODS

In Sec. IV C, the ν_2 and ν_3 bands of crystalline CO_2 particles are modeled using the bulk optical properties of cubic CO_2 and classical electrostatics.[22] The dielectric function of CO_2 was constructed using the following expression:

$$\epsilon(\omega) = \epsilon'(\omega) + i\epsilon''(\omega), \tag{1}$$

where

$$\epsilon'(\omega) = \epsilon_\infty \left(1 + \sum_{m=1}^{N} \frac{\left(\omega_{L_m}^2 - \omega_{T_m}^2\right)\left(\omega_{T_m}^2 - \omega^2\right)}{\left(\omega_{T_m}^2 - \omega^2\right)^2 + (\omega\gamma_m)^2}\right), \tag{2}$$

$$\epsilon''(\omega) = \epsilon_\infty \sum_{m=1}^{N} \frac{\left(\omega_{L_m}^2 - \omega_{T_m}^2\right)(\omega\gamma_m)}{\left(\omega_{T_m}^2 - \omega^2\right)^2 + (\omega\gamma_m)^2}. \tag{3}$$

The number of optical modes was set to three ($N = 3$). The transverse optical (TO) frequencies (ω_T) of these modes were 655, 661, and 2345 cm^{-1} with corresponding longitudinal optical (LO) frequencies (ω_L) at 660, 672, and 2377 cm^{-1}, respectively. These modes were based on a fit to refractive index data from a thin film study.[23] The high-frequency dielectric constant was also taken from that work ($\epsilon_\infty = 1.54$). When calculating spectra, the damping of each mode (γ_m) is listed in the corresponding figure caption.

All modes and spectra were calculated within the electrostatic approximation. With this approach, the wavelength of light is assumed to be much larger than any of the particle dimensions that it is impinging on.[22] This limit is satisfied for all of the experimentally prepared particles that are considered here. One advantage of using this method is that, in some cases, analytical expressions for the surface modes of an object can be derived. This allows for the concise evaluation of the surface modes over all possible parameters that define an object. The objects considered here are (i) a spherical shell, (ii) a prolate and oblate ellipsoid, and (iii) clusters of spherical particles. These are used as models for the three types of particles that are of experimental interest: (i) core-shell particles, (ii) various elongated or anisotropic particles, and (iii) clusters of closely spaced particles.

Surface modes were determined by examining the expression that defines the polarizability of an object in a uniform electric field. The frequency at which the denominator of the polarizability vanishes corresponds to a surface mode. In the limit of the electrostatic approximation, these surface modes dominate the absorption spectrum of an object. For spherical shells and ellipsoids polarizability expressions are well known.[22] In the case of a spherical shell with an inner radius of a and an outer radius of b the condition that the dipole modes satisfy is

$$(\epsilon(\omega) + 2\epsilon_m)(\epsilon_c + 2\epsilon(\omega)) + (a/b)^3(2\epsilon(\omega) - 2\epsilon_m)(\epsilon_c - \epsilon(\omega)) = 0, \tag{4}$$

where ϵ_c and ϵ_m are the dielectric functions for the core and medium, respectively. In all calculations these were simply set to one. For an ellipsoid, dipole modes satisfy

$$3\epsilon_m + 3L(\epsilon(\omega) - \epsilon_m) = 0, \tag{5}$$

where the geometrical factor L is dependent on whether or not the ellipsoid is oblate or prolate, the direction of the incident polarization of light, and the length of the various ellipsoidal axes. Expressions for this factor are given in Ref. 22.

For clusters of spheres, analytical expressions only exist for a few simple arrangements.[24] In more complicated situations, which are of interest here, a more general method needs to be used. This can be developed as follows: in a distribution of spheres the dipole moment of each sphere is

$$\mathbf{P}_i = \epsilon_m \alpha_i \mathbf{E}_{\mathrm{loc}}(\mathbf{r}_i), \tag{6}$$

where $\mathbf{E}_{\mathrm{loc}}(\mathbf{r}_i)$ is the electric field at sphere i and the polarizability of each sphere, α_i, is

$$\alpha_i = 4\pi a_i^3 \frac{\epsilon(\omega) - \epsilon_m}{\epsilon(\omega) + 2\epsilon_m}, \tag{7}$$

where a_i is the radius of the sphere. In the absence of an external field, a system of coupled equations for N spheres can be defined by

$$\mathbf{P}_i = \epsilon_m \alpha_i \sum_{j \neq i}^{N} \mathbf{A}_{ij} \mathbf{P}_j, \tag{8}$$

where

$$\mathbf{A}_{ij} = \frac{1}{4\pi\epsilon_m} \frac{(3\hat{\mathbf{r}}_{ij}\hat{\mathbf{r}}_{ij} - \mathbf{I})}{|\mathbf{r}_{ij}|^3}, \tag{9}$$

and $\mathbf{r}_{ij}$ is the center-to-center distance vector between spheres i and j, $\hat{\mathbf{r}}_{ij}$ is the corresponding unit vector, and $\mathbf{I}$ is a 3×3 identity matrix.

The system of equations generated by Eq. (8) can be written as an eigenvalue problem in the form of

$$\mathbf{BP} = \Lambda \mathbf{P}, \tag{10}$$

where

$$\Lambda = \frac{\epsilon(\omega) + 2\epsilon_m}{\epsilon(\omega) - \epsilon_m}, \tag{11}$$

and the elements of $\mathbf{B}$ are defined by

$$\mathbf{B}_{ij} = \begin{cases} 0, & i = j \\ 4\pi\epsilon_m a_i^3 \mathbf{A}_{ij}, & i \neq j \end{cases}. \tag{12}$$

Although there are $3N$ modes in a system of N spheres, only the strongest optically active modes are considered here (these have been called "in-phase" modes for one-dimensional assemblies).[24] These modes can easily be determined by examining the dipole moments from an eigenvector **P**. It is important to note that other modes (associated with higher order moments) can be important in systems of clustered spheres even if the overall dimensions of the cluster satisfies the electrostatic limit.[25] Therefore, several calculations using the above approach were compared to results obtained using Mie theory for coupled spheres.[26] The differences between the coupled Mie theory and electrostatic calculations were found to be minor and, as an approximation, the electrostatic results were judged to be satisfactory.

IV. RESULTS AND DISCUSSION

A. Pure CO_2 and pure C_2H_2 aerosols

Prior to considering aerosol particles composed of the $CO_2 \cdot C_2H_2$ co-crystal, we first summarize the results for pure C_2H_2 (Fig. 1(a)) and pure CO_2 (Fig. 1(g)) aerosols. Our recent study on C_2H_2 aerosols revealed that pure C_2H_2 preferentially forms orthorhombic, polycrystalline particles under conditions similar to those studied here.[27] This polycrystalline phase makes analysis of the particle shape through the examination of the IR active fundamental modes—the ν_5 bend and the ν_3 anti-symmetric stretch—difficult (see Ref. 27 for a discussion on this issue). However, these polycrystalline particles are likely globular in shape.[27] The bands also show little change in shape over time, suggesting that the particles retain their globular shape over the course of the measurements. In the C_2H_2 orthorhombic phase, the ν_5 vibration has three optical modes and the ν_3 vibration has two optical modes. For a particle that is roughly spherical in shape there should therefore be three peaks for the ν_5 band and two peaks for ν_3 band. For the ν_5 band, the approximate locations of the three peaks are indicated in Fig. 1(a), although the polycrystalline nature of the material makes a precise assignment difficult as the peaks overlap more so than those of the pure crystal. For the ν_3 band, the frequencies of the two optical modes are nearly identical (see Part II). Therefore, only one observable peak is expected for this band. Its location is also indicated in Fig. 1.

Pure CO_2 aerosols have been extensively studied,[28–37] and the particles formed under the conditions used here have the same cubic crystal structure as bulk, crystalline CO_2 for similar temperatures (T = 78 K). When studying particles of this phase it is important to note that the two IR active fundamental modes of CO_2—the ν_2 bend and the ν_3 anti-symmetric stretch—possess significant LO-TO splittings. Consequently, the peaks found in these bands will have a strong dependence on particle shape. This effect has its molecular origin in strong transition dipole coupling (vibrational exciton coupling).[35,38,39] As we have discussed and verified by modeling in previous publications,[34,36] the time evolution of these bands is the result of a shape change from cube-like particles to particles with increasingly elongated shapes. The ν_3 band of the cube-like particles features a strong central peak (2361.0 cm^{-1}) with a weak, higher energy side peak (2371.2 cm^{-1}). In the case of elongated particles, a lower energy peak dominates the spectra while a smaller, higher energy peak remains. This lower energy peak is already present in Fig. 1(g) at 2346.9 cm^{-1}. At longer times the absorbance of this peak increases relative to the other peaks in this band. The smaller LO-TO splittings found in the optical modes of the CO_2 ν_2 vibration means that shape-dependent features are more compressed than in the ν_3 band. However, the overall band shapes are similar to those found in the ν_3 band. In Fig. 1, only the dominant peaks for each optical mode are indicated.

B. $CO_2 \cdot C_2H_2$ aerosols immediately after formation

The initial formation of the $CO_2 \cdot C_2H_2$ co-crystal in the aerosol phase was confirmed through the examination of the positions of several of the fundamental and combination bands of both C_2H_2 and CO_2 (Figs. 1(b)–1(f)) and the modeling of IR spectra (Part II). Note that all of these spectra show features arising from pure CO_2 and pure C_2H_2 in addition to the features from the co-crystalline phase. Relative to their positions in the respective spectra of the pure aerosols (Fig. 1(a) for pure C_2H_2 and Fig. 1(g) for pure CO_2), the C_2H_2 ν_3 band was shifted by +28.5 cm^{-1} while the CO_2 ^{13}C-ν_3, $2\nu_2 + \nu_3$, and $\nu_1 + \nu_3$ bands were shifted by −5.3, −11.4, and −9.8 cm^{-1}, respectively. The wavenumbers of these peaks are consistent with what has been reported by Gough *et al.* for the $CO_2 \cdot C_2H_2$ co-crystal,[17–19] confirming the formation of the same $CO_2 \cdot C_2H_2$ phase that was found in the thin films from that work. For the optical modes with larger LO-TO splittings in their pure crystalline phases (the CO_2 ν_2 and C_2H_2 ν_5 bands), the band positions of the $CO_2 \cdot C_2H_2$ aerosol differ somewhat from those reported by Gough *et al.* for thin films. This difference is almost certainly due to a dependence

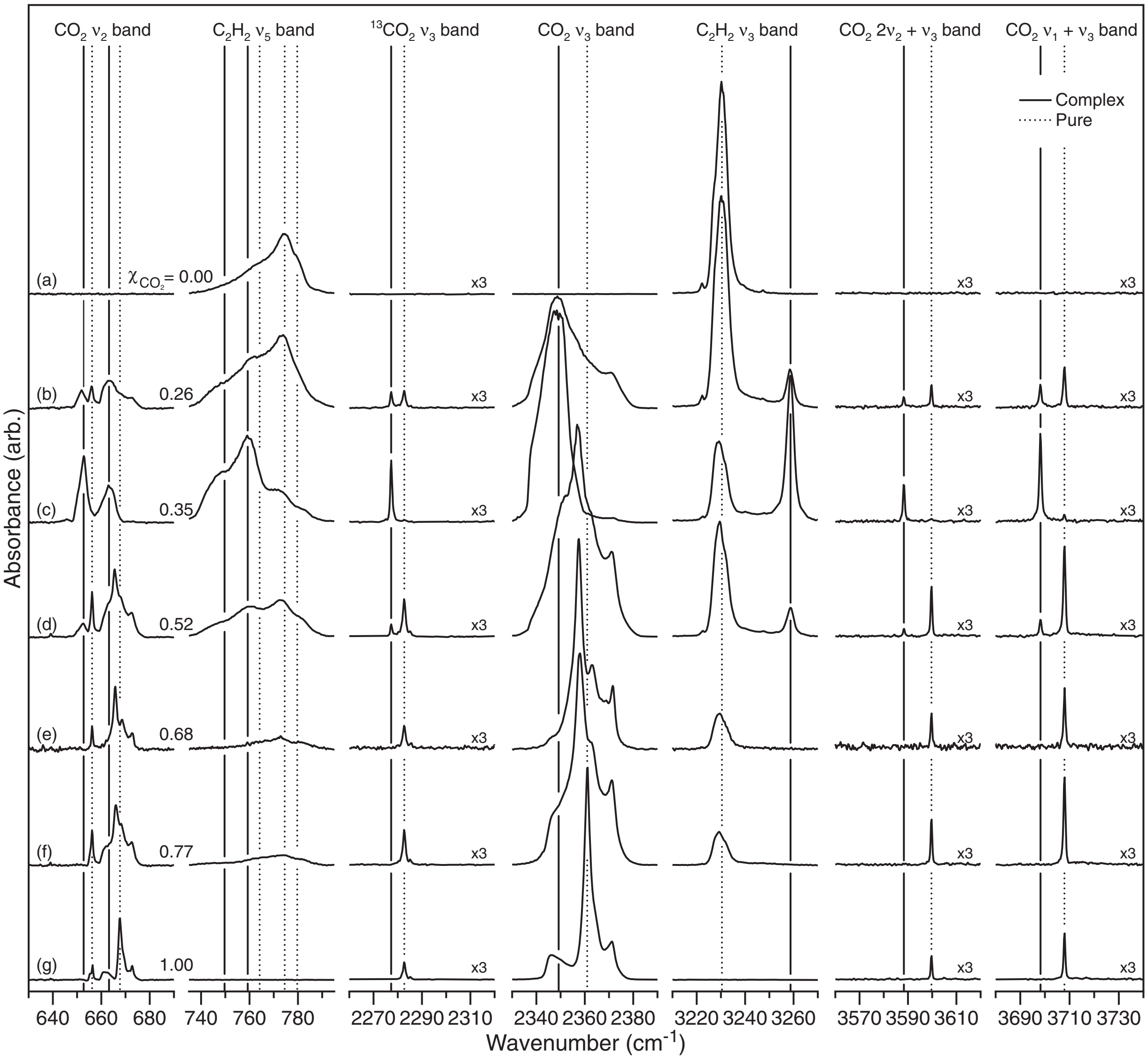

FIG. 1. Experimental IR spectra for aerosols composed of CO_2 and C_2H_2 mixed in various ratios. The mole fraction of CO_2 present in each sample is indicated next to its corresponding trace. The location of peaks associated with pure CO_2 and pure C_2H_2 are indicated with a dashed line while the location of peaks associated with $CO_2 \cdot C_2H_2$ are indicated with a solid line. Details of the exact composition of (a) through (g) are summarized in Table I. All spectra are recorded at time t = 0 s.

of band positions on particle shape, indicating that a large LO-TO splitting is also present in the $CO_2 \cdot C_2H_2$ phase. The role of this effect is discussed in detail in the subsequent paper (Part II). A large LO-TO splitting should also be present in the CO_2 ν_3 band of the co-crystal which, in the cubic CO_2 phase, has the largest LO-TO splitting of any of the modes discussed here. However, this band is not discussed by Gough *et al.* so there is no thin film reference for comparison (presumably this band was saturated in their spectrum).

In Fig. 1, the mole fraction of injected CO_2 is indicated on each trace and Table I lists the mole fractions of the pure and complexed (co-crystalline) components for each trace. All of these fractions were calculated using the relative absorbance intensities of the C_2H_2 ν_3 band and the CO_2 $\nu_1 + \nu_3$ band for both the pure and complexed substances. These intensities were converted into mole fractions using the relative extinction coefficients calculated by Gough *et al.*[18]

Figure 1 and Table I both show that while it was possible to prepare $CO_2 \cdot C_2H_2$ aerosols with nearly no pure CO_2 (Fig. 1(c)) it was not possible to prepare $CO_2 \cdot C_2H_2$ aerosols without a significant amount of pure C_2H_2. This is true even

TABLE I. Mole fractions of the injected gases and of the components present in the mixed $CO_2 \cdot C_2H_2$ aerosols.

	Injected fraction		Aerosol fraction			
	χ_{CO_2}	$\chi_{C_2H_2}$	χ_{CO_2} pure	χ_{CO_2} complexed	$\chi_{C_2H_2}$ pure	$\chi_{C_2H_2}$ complexed
a	0.00	1.00	0.00	0.00	1.00	0.00
b	0.26	0.74	0.18	0.08	0.64	0.10
c	0.35	0.65	0.03	0.32	0.28	0.37
d	0.52	0.48	0.46	0.06	0.40	0.08
e	0.68	0.32	0.67	0.01	0.30	0.02
f	0.77	0.23	0.76	0.01	0.22	0.01
h	1.00	0.00	1.00	0.00	0.00	0.00

for the cases where a slight (Fig. 1(d)) or large (Figs. 1(e) and 1(f)) excess of CO_2 is injected. Despite the expectation that all of the C_2H_2 would be complexed in these situations, there is actually a *decrease* in the amount of $CO_2 \cdot C_2H_2$ relative to the total amount of C_2H_2 present. This result is similar to what was reported by Gough *et al.*[18] In that work, the authors speculated that pure, crystalline CO_2, which will simultaneous be formed when an excess of CO_2 is used, inhibits the formation of the $CO_2 \cdot C_2H_2$ phase.[18] This type of effect also occurs when attempting to use an excess of C_2H_2 to ensure that all of the CO_2 is complexed, although it is not as significant (compare the amount of complexed $CO_2 \cdot C_2H_2$ present in Fig. 1(c) with Fig. 1(e)). In this case, pure C_2H_2 would need to inhibit the formation of the $CO_2 \cdot C_2H_2$ phase.

A surprising result is that the equimolar mixture of CO_2 and C_2H_2 (Fig. 1(d)) contained such a large fraction of pure components relative to those that are complexed. This differs from Gough *et al.* where the spraying of equimolar mixtures led to the nearly exclusive formation of $CO_2 \cdot C_2H_2$ in thin films.[18] Therefore, the injection of equimolar mixtures into the bath cooling cell was investigated further. It was found that when the pressure of the gas mixture was increased, so too did the amount of co-crystalline $CO_2 \cdot C_2H_2$ that initially formed. For instance, when this pressure was doubled from the conditions used in Fig. 1, a three- to four-fold increase in the amount of $CO_2 \cdot C_2H_2$ formed in the aerosol occurred (spectra not shown). An explanation for this dependence may lie in the formation kinetics of the co-crystalline phase. However, these kinetics were not studied in detail. Finally, an analysis of the co-crystalline phase with a 1:1 mixing ratio of C_2H_2:CO_2 is provided in Part II.

C. $CO_2 \cdot C_2H_2$ aerosols after the decomposition of the $CO_2 \cdot C_2H_2$ co-crystalline phase

1. Overview

Similar to Gough *et al.*, we observed the decomposition of the co-crystalline $CO_2 \cdot C_2H_2$ phase into pure C_2H_2 and pure CO_2 in all of the prepared $CO_2 \cdot C_2H_2$ aerosols (over a time period of about 12 min). Figure 2 shows spectra of $CO_2 \cdot C_2H_2$ aerosols recorded at different times during decomposition. The mole fraction of injected CO_2 for this sample is 0.35. We focus on this sample as, of all the aerosols that were prepared, it contained the largest mole fraction of co-crystalline $CO_2 \cdot C_2H_2$ (Table I). Over the period of time studied in Fig. 2 the decomposition of $CO_2 \cdot C_2H_2$ proceeds to near completion. In this section, we focus on the analysis of the IR spectra of the decomposed aerosols at t = 730 s. As the optical properties of the crystalline phases of pure CO_2 and pure C_2H_2 under similar conditions have been previously studied (Sec. IV A), this is simpler than studying the aerosols immediately after formation (studied in Part II) or prior to the completion of decomposition.

As the decomposition of co-crystalline $CO_2 \cdot C_2H_2$ proceeds, so too must the phase separation of pure CO_2 and pure C_2H_2 in the aerosol particles. Gough *et al.* hypothesized that this process results in the formation of "microcrystallites of CO_2 embedded in a softer, deformed matrix of C_2H_2."[19] One interpretation of this type of structure, for aerosol particles, is depicted in Fig. 3(a). However, there exist many other possible architectures aside from this. For example, core-shell structures (Figs. 3(b) and 3(c)). As these structures can in principle be experimentally prepared through the sequential injection of C_2H_2 and CO_2, it is straightforward to compare the decomposed aerosol spectra to those of actual core-shell particles. These results will aid in characterizing the decomposed products.

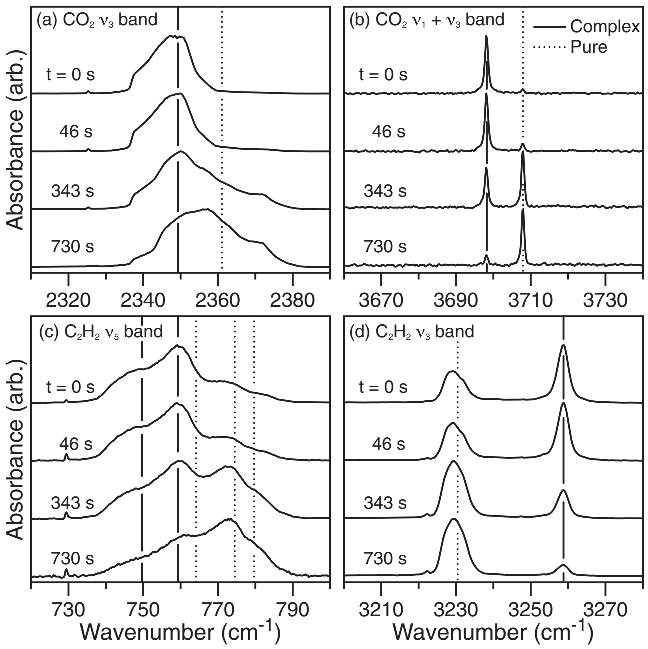

FIG. 2. Time-dependent IR spectra for an aerosol composed of CO_2 and C_2H_2. The mole fraction of CO_2 is 0.35.

Figure 4 compares the spectra of core-shell structures prepared through the sequential injection of the pure components to the spectrum of the decomposed (t = 730 s) aerosols. Two different types of core-shell particles were prepared: (i) CO_2 shell–C_2H_2 core particles (Fig. 4(b)) and (ii) C_2H_2 shell–CO_2 core particles (Fig. 4(c)). As expected the C_2H_2 ν_5 and ν_3 bands give little information on particle architecture. For these bands, shapes and peak positions across Figs. 4(a)–4(c) are too similar to allow for any differen-

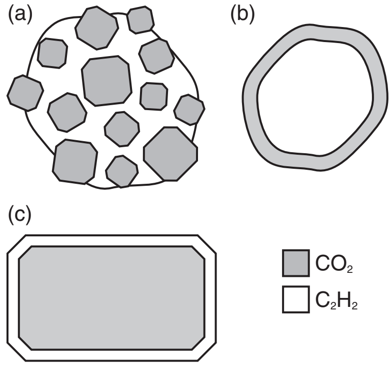

FIG. 3. Diagrams for possible architectures of aerosol particles after decomposition of the co-crystalline $CO_2 \cdot C_2H_2$ phase: (a) CO_2 domains embedded in a C_2H_2 matrix, (b) CO_2 shell on a C_2H_2 core, and (c) C_2H_2 shell on a CO_2 core.

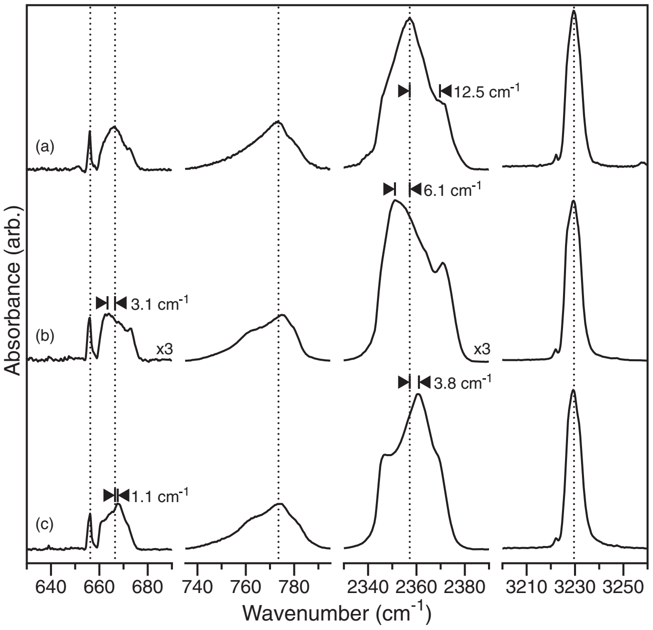

FIG. 4. Comparison between experimental IR spectra of (a) decomposed $CO_2 \cdot C_2H_2$ aerosols (t = 730 s in Fig. 2), (b) CO_2 shells formed on a C_2H_2 core (note the scale factor of three for the CO_2 bands), and (c) C_2H_2 shells formed on a CO_2 core. As the decomposition of $CO_2 \cdot C_2H_2$ in (a) was not 100% complete (see Fig. 2 at t = 730 s), small bands associated with residual co-crystalline $CO_2 \cdot C_2H_2$ were subtracted using an appropriate $CO_2 \cdot C_2H_2$ spectrum.

tiation between the various aerosols. The CO_2 bands, by contrast, show distinct differences in band shapes and peak positions. Examination of the CO_2 ν_3 band of the two core-shell structures that were prepared (Figs. 4(b) and 4(c)) reveals that, in terms of overall band shape, the spectrum of the CO_2 shell–C_2H_2 core structure apparently provides the better match to Fig. 4(a). However, the position of the dominant peak in the spectrum of the C_2H_2 shell–CO_2 core structure (2361.0 cm^{-1}) shows slightly better agreement with that of the decomposed aerosol (2357.2 cm^{-1}) than that of the CO_2 shell–C_2H_2 core (2351.1 cm^{-1}). As discussed in Sec. IV A, all of the shape-dependent information that is found in the ν_3 band is also present in ν_2 band. However, due to the smaller LO-TO splitting it is more compressed. Therefore, throughout the remaining discussion we focus entirely on the CO_2 ν_3 band.

2. *CO_2 shells with C_2H_2 cores*

For CO_2 shells, the sensitivity of peak positions to shell thickness was studied previously.[40] It is possible that the difference in peak positions between the CO_2 bands of Figs. 4(a) and 4(b) is a consequence of a small difference in thickness. Note that the mole fraction of CO_2 is smaller in the aerosol whose spectrum is shown in Fig. 4(b) than the aerosol whose spectrum is shown in Fig. 4(a). This means that, in this case, shells prepared through sequential injection are thinner than any shells formed through decomposition of the $CO_2 \cdot C_2H_2$ phase.

When dealing with the IR absorption spectra of dielectric shells, it is well known that for constant core size an increase in the shell thickness causes the splitting between the two dominant absorption peaks to decrease.[40] Therefore, it is possible that the CO_2 shells whose spectrum is shown in Fig. 4(b) are too thin to give a good match to the spectrum in Fig. 4(a). Unfortunately, experimental attempts to prepare thicker shells through sequential injection were unsuccessful. Simply increasing the mole fraction of injected CO_2 in order to prepare thicker shells resulted in spectra which were best characterized as being a mixture of pure CO_2 particles and CO_2 shell–C_2H_2 core particles. Therefore, the possibility of thicker shells was explored through calculations using the analytical expressions for the surface modes of a spherical shell. These calculations allow the ratio of CO_2 to C_2H_2 to be easily varied.

For the spherical shell, the two surface modes of the CO_2 ν_3 band are plotted on the left side of Fig. 5 as a function of the scale parameter b/a, where b is the radius of the outer sphere and a is the radius of the inner sphere. On the right side of Fig. 5 the calculated spectrum for a ratio of $b/a = 1.26$ illustrates where two of these surface modes would be found in a spectrum. Next, we assume that the spectrum in Fig. 4(b) is that of a spherical shell whose core and shell volumes are determined by the amount of injected C_2H_2 and CO_2, respectively. When the molar volumes for cubic CO_2 and orthorhombic C_2H_2 are used,[14,15] this assumption yields a scale parameter of $b/a = 1.08$. In order for the lower energy surface mode in Fig. 5 to shift by 6.1 cm^{-1} (similar to what is observed when going from Fig. 4(b) to 4(a)), b/a would need to change from 1.08 to 1.47. Such a change would require that the mole fraction of CO_2 present in the aerosol increase from 0.24 to 0.72. When moving from Fig. 4(b) to 4(a), the actual increase is from 0.24 to 0.35. Such a large discrepancy between the modeled and experimental results means that the formation of a CO_2 shell-like structure through decomposition is unlikely. Even if other factors are taken into consideration with this model (e.g., using a shell model that is non-spherical or altering the dielectric constant of the core), the requirements of using CO_2 shells to account for the band shapes in Fig. 4(a) will always demand differences in thicknesses that far exceed experimental errors. Therefore, this structure seems unlikely.

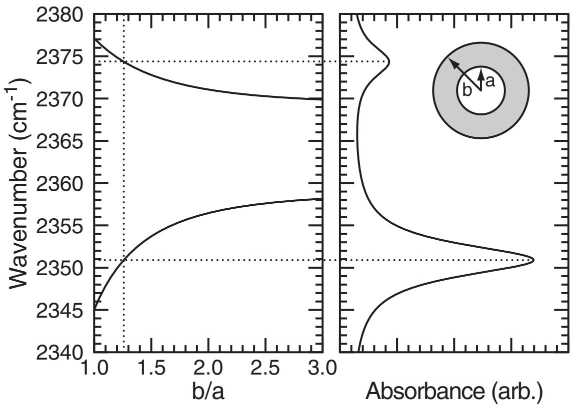

FIG. 5. Left side: position of surface modes for the ν_3 band of a spherical CO_2 shell. These modes are plotted as a function of the outer radius, b, divided by the inner radius, a. Right side: a sample spectrum for $b/a = 1.26$. For the calculated spectrum, the damping constant in the dielectric function was set to 0.2% of ω_T.

3. C_2H_2 shells with CO_2 cores

Next, we consider whether or not the spectrum of the C_2H_2 shell–CO_2 core (Fig. 4(c)) can be reconciled with that of Fig. 4(a). As discussed in Sec. IV A, when pure CO_2 is injected into the cell the shape of the CO_2 ν_2 and ν_3 bands show a strong temporal dependence believed to originate from the formation and growth of elongated particles. In the sequential injection of CO_2 followed by C_2H_2 it was found that this type of evolution would halt once C_2H_2 was injected. This was presumed to be due to the coating of CO_2 particles with C_2H_2. During the decomposition of the co-crystalline $CO_2 \cdot C_2H_2$ phase, any growth of CO_2 particles inside a C_2H_2 matrix would be similarly blocked. However, obtaining experimental IR spectra similar to the one in Fig. 4(a) using a sequential injection method again proved difficult. The main discrepancy is that the low energy peak at 2346.9 cm^{-1} in Fig. 4(c) is not found in Fig. 4(a). As the position of this lower energy mode is very sensitive to the aspect ratio of the elongated particle, it is possible that the aspect ratio of the particles whose spectrum is shown in Fig. 4(c) is simply too large in comparison to the particles whose spectrum is shown in Fig. 4(a). If the aspect ratio was decreased the low energy peak, located at 2346.9 cm^{-1} in Fig. 3(c), could shift into the region between 2355 and 2361 cm^{-1}. This would lead to a better correspondence with Fig. 3(a).

As it was difficult to experimentally produce particles with specific aspect ratios, the influence of this parameter was modeled using the electrostatic solution to an ellipsoid.[22] Rod-like particles were modeled using a prolate spheroid (Figs. 6(a) and 6(b)) while disc-like particles were modeled using an oblate spheroid (Figs. 6(c) and 6(d)). The pure CO_2 aerosol whose spectrum was shown in Fig. 1(g) primarily consists of cube-like particles (i.e., not elongated). Within this ellipsoidal model, these can be taken as a reference for particles with an aspect ratio of one. For the CO_2 ν_3 band, the difference in peak position between the dominant peak in the spectrum shown in Fig. 1(g) and that of Fig. 4(a) is about 3.8 cm^{-1}. For the rod-like particles, such a change occurs when the aspect ratio is increased from 1 to 1.5, while for the disc-like particles the aspect ratio needs to increase from 1 to 2.1. The spectra for these two aspect ratios are plotted in Figs. 6(b) and 6(d), respectively. For the disc-like particle, the ratio of peak heights associated with the two ellipsoidal modes fits much better to the experimental spectrum in Fig. 4(a) than the rod-like particle shape. Furthermore, the splitting between the two surface modes of the disc-like ellipsoid (10.6 cm^{-1}) shows a better correspondence to the observed splitting of 12.5 cm^{-1} than the rod-like ellipsoid (5.5 cm^{-1}). Therefore, disc-like CO_2 particles with an axis ratio of around 2.1 coated with C_2H_2 could explain the spectrum in Fig. 4(a).

4. CO_2 domains in a C_2H_2 matrix

Next, we consider the possibility that the aerosol particles resemble the situation shown in Fig. 3(a). Unlike the case of the core-shell particles, where sequential injection provides a means to experimentally produce the structures depicted in Figs. 3(b) and 3(c), there is no obvious experimental method that allows for the direct formation of a particle similar in structure to Fig. 3(a). Therefore, we have to rely entirely on modeling for such particles. As a model we use clusters/assemblies of spherical CO_2 particles. Figure 7 shows the wavenumbers of the strongest optically active modes for one-, two-, and three-dimensional assemblies of spheres. As discussed in Sec. III, these modes dominate the spectrum when a cluster of spheres is much smaller than the wavelength of light impinging on it.

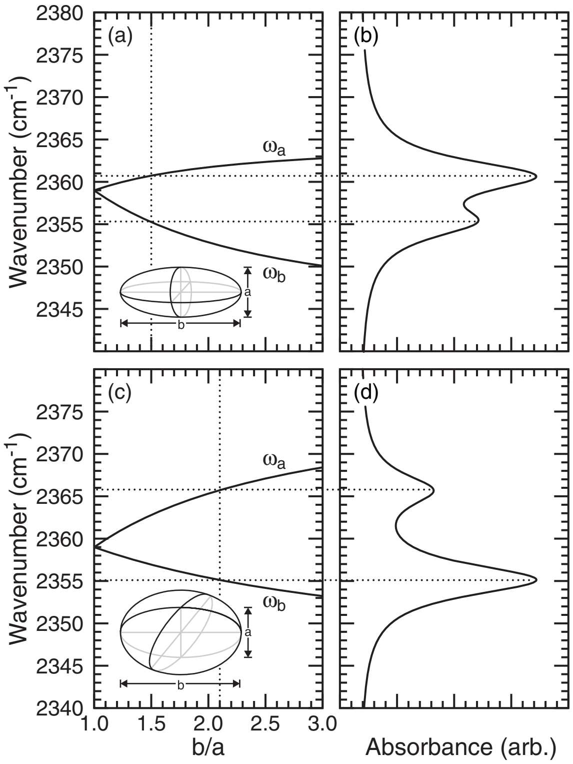

FIG. 6. (a) Position of the surface modes for the ν_3 band of a prolate CO_2 spheroid (rod-like particle). (b) A sample spectrum for a prolate CO_2 spheroid defined by $b/a = 1.5$. (c) Position of surface modes for the ν_3 band of an oblate CO_2 spheroid (disc-like particle). (d) A sample spectrum for an oblate CO_2 spheroid defined by $b/a = 2.1$. For the calculated spectra, the damping constant in the dielectric function was set to 0.2% of ω_T.

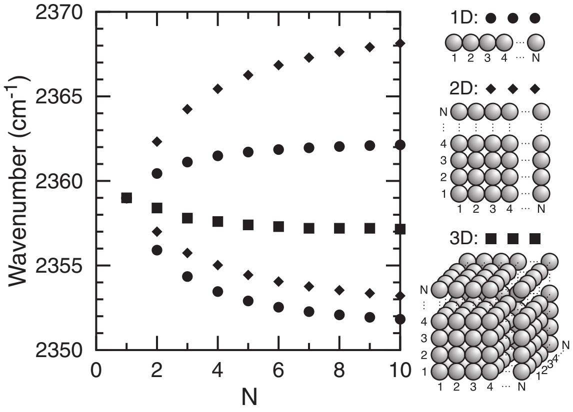

FIG. 7. Position of the dominant optically active modes for one-, two- and three-dimensional assemblies of CO_2 spheres. As the three-dimensional assemblies contain many optically active modes only the position of the dominant peak of each overall spectrum is listed.

The one- and two-dimensional examples in Fig. 7 illustrate that interparticle coupling can easily account for the difference in peak position between an isolated particle (Fig. 1(g)) and a system that potentially contains particles that are clustered together (Fig. 4(a)). Furthermore, the band shape of the two-dimensional structure (not shown) is very similar to that of the disc-like ellipsoid, which was shown to have a good correspondence to the shape in Fig. 4(a). However, the ordered structures in Fig. 7 are not satisfactory models of the particle depicted in Fig. 3(a). Placing the spheres into random positions within a large geometric domain (representing the C_2H_2 matrix) is a more suitable approach. This was examined by randomly packing CO_2 spheres into either (i) a larger C_2H_2 sphere or (ii) a larger C_2H_2 cube. These larger structures had dimensions that were 10 to 20 times the radii of the spheres packed inside. When spheres were packed inside at low densities the CO_2 bands resembled that of isolated CO_2 spheres while at high packing densities CO_2 spectra began to resemble those of the domain that the randomly placed spheres were chosen to fill. Therefore, unless these spheres are tightly packed into a disc-like structure, they will not be able to account for the overall band shape and peak position observed in Fig. 4(a). This means that a particle model similar to that depicted in Fig. 3(a) is unlikely as a random distribution of separated CO_2 crystallites is insufficient to cause the observed shift.

For completeness we also consider the opposite situation: C_2H_2 domains embedded inside a CO_2 matrix (i.e., the materials in Fig. 3(a) are interchanged). The formation of such particles under these experimental conditions is problematic for two reasons. First, such a growth process would be inconsistent with the study presented by Gough *et al.*[19] In that work, kinetic data were shown to fit very well with a model of CO_2 domains growing inside of a C_2H_2 matrix. Second, the mole fraction of CO_2 present in the aerosols whose spectrum is shown in Fig. 4(a) is 0.35. This gives a total volume of CO_2 present in a particle consisting of domains of pure CO_2 and pure C_2H_2 of about 31%. Such a small volume would mean that the C_2H_2 domains would be very densely packed inside such a particle. This would lead to situations where the CO_2 matrix is broken up into smaller domains throughout the particle. In this case, the above analysis concerning CO_2 domains inside a C_2H_2 matrix would again be valid. As was already discussed, the optical properties of this structure are not consistent with the spectrum shown in Fig. 4(a).

5. Summary of analysis

Based on the above analysis, the modeled spectra of disc-like ellipsoids consisting of a CO_2 core and a C_2H_2 shell provides the best match to the observed CO_2 bands of the decomposed $CO_2 \cdot C_2H_2$ aerosols (Fig. 4(a)). The observed and modeled spectra of these particles are shown in Fig. 8. No attempt was made to model a distribution of ellipsoids or structural changes at the CO_2-C_2H_2 interface although this undoubtedly plays an important role in some of the discrepancies between the two spectra. Including either of these effects would broaden the bands in the calculated spectra. The satisfactory correspondence between the spectrum of the disc-like ellipsoid and the experimental spectrum does not necessarily mean that the CO_2 domains are perfectly ellipsoidal, but rather they can be described as being roughly disc-like.

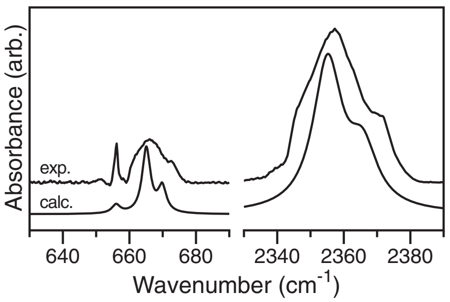

FIG. 8. Comparison between experimental (Fig. 4(a)) and modeled spectra after decomposition of the originally co-crystalline $CO_2 \cdot C_2H_2$ particles. The modeled spectrum is that of an oblate CO_2 spheroid (disc-like particle) with $b/a = 2.1$. Damping was set to 0.45% of ω_T for each mode.

Overall, this type of structure is also consistent with the decomposition mechanism proposed and modeled by Gough *et al.* (CO_2 particles in a deformed C_2H_2 matrix). The hypothesis of a C_2H_2 shell on a CO_2 core is also physically reasonable given the previous observations that, under these experimental conditions, the C_2H_2 phase is disordered and deformable while the CO_2 phase is always crystalline. Furthermore, the small aspect ratios mean that this model does not require the formation of particles with unrealistic aspect ratios during decomposition (e.g., it would only require the coalescence of several roughly spherical crystallites of CO_2 inside a C_2H_2 matrix). Finally, from Fig. 6 it can be seen that the sensitivity of the peak position to the aspect ratio in this region is small, so the presence of a distribution of particles with varying ratios would not be expected to produce a completely broadened, unstructured peak. This is also consistent with what is observed.

V. SUMMARY

In the present work, we have investigated the mid-IR spectra of aerosol particles composed of mixed CO_2 and C_2H_2 with various compositions and architectures at cryogenic temperatures. For aerosol particles formed by co-condensation of CO_2 and C_2H_2 we have found the same $CO_2 \cdot C_2H_2$ co-crystalline phase that had previously been observed in thin films.[17–19] An analysis of this co-crystalline phase is provided in the subsequent paper (Part II). Similar to the thin films, the co-crystalline particles were found to be metastable and decomposed into pure CO_2 and pure C_2H_2 over time. The architecture of the particles after decomposition was analyzed. From the different particle architectures that were proposed, disc-like $CO_2 \cdot C_2H_2$ core-shell ellipsoids with an aspect ratio of approximately 2.1 seem to be the most consistent with the experimentally observed aerosol particles after decomposition.

ACKNOWLEDGMENTS

Financial support from the Natural Sciences and Engineering Research Council of Canada (NSERC) and the

Canada Foundation for Innovation is gratefully acknowledged. This research has been enabled through the generous allocation of advanced computer resources by WestGrid and Compute/Calcul Canada. T.C.P. acknowledges a NSERC fellowship and R.S. acknowledges a NSERC E. W. R. Steacie memorial fellowship.

[1] P. A. Gerakines, W. A. Schutte, J. M. Greenberg, and E. F. van Dishoeck, Astron. Astrophys. **296**, 810 (1995).
[2] R. Courtin, Space Sci. Rev. **116**, 185 (2005).
[3] S. K. Atreya, E. Y. Adams, H. B. Niemann, J. E. Demick-Montelara, T. C. Owen, M. Fulchignoni, F. Ferri, and F. Wilson, Planet. Space Sci. **54**, 1177 (2006).
[4] R. de Kok, P. G. J. Irwin, N. A. Teanby, C. A. Nixon, D. E. Jennings, L. Fletcher, C. Howett, S. B. Calcutt, N. E. Bowles, F. M. Flasar, and F. W. Taylor, Icarus **191**, 223 (2007).
[5] C. C. Wang, P. Zielke, Ó. F. Sigurbjörnsson, C. R. Viteri, and R. Signorell, J. Phys. Chem. A **113**, 11129 (2009).
[6] A. Määttänen, F. Montmessin, B. Gondet, F. Scholten, H. Hoffmann, F. González-Galindo, A. Spiga, F. Forget, E. Hauber, G. Neukum, J.-P. Bibring, and J.-L. Bertaux, Icarus **209**, 452 (2010).
[7] P. Forster, V. Ramaswamy, P. Artaxo, T. Berntsen, R. Betts, D. W. Fahey, J. Haywood, J. Lean, D. C. Lowe, G. Myhre, J. Nganga, R. Prinn, G. Raga, M. Schulz, and R. V. Dorland, "Changes in atmospheric constituents and in radiative forcing," in *Climate Change 2007: The Physical Science Basis. Contribution of Working Group I to the Fourth Assessment Report of the Intergovernmental Panel on Climate Change*, edited by S. Solomon, D. Qin, M. Manning, Z. Chen, M. Marquis, K. B. Averyt, M. Tignor, and H. L. Miller (Cambridge University Press, Cambridge, New York, 2007).
[8] P. Ehrenfreund, H. J. Fraser, J. Blum, J. H. E. Cartwright, J. M. Garcia-Ruiz, E. Hadamcik, A. C. Levasseur-Regourd, S. Price, F. Prodi, and A. Sarkissian, Planet. Space Sci. **51**, 473 (2003).
[9] C. P. McKay, A. Coustenis, R. E. Samuelson, M. T. Lemmon, R. D. Lorenz, M. Cabane, P. Rannou, and P. Drossart, Planet. Space Sci. **49**, 79 (2001).
[10] M. H. Moore, R. L. Hudson, and R. F. Ferrante, Earth, Moon, Planets **92**, 291 (2003).
[11] V. J. Herrero, Ó. Gálvez, B. Maté, and R. Escribano, Phys. Chem. Chem. Phys. **12**, 3164 (2010).
[12] M. T. Kirchner, D. Bläser, and R. Boese, Chem. Eur. J. **16**, 2131 (2010).
[13] N. Fray and B. Schmidt, Planet. Space Sci. **57**, 2053 (2009).
[14] R. W. G. Wyckoff, *Crystal Structures* (Wiley, New York, 1963).
[15] R. K. McMullan, Å. Kvick, and P. Popelier, Acta Crystallogr. B **48**, 726 (1992).
[16] C. G. Gray and K. E. Gubbins, *Theory of Molecular Fluids: Fundamentals* (Clarendon, Oxford, 1984), Vol. 1.
[17] T. E. Gough and T. E. Rowat, J. Chem. Phys. **102**, 3932 (1995).
[18] T. E. Gough and T. E. Rowat, J. Chem. Phys. **109**, 6809 (1998).
[19] T. E. Gough, T. E. Rowat, and R. Illner, Chem. Phys. Lett. **298**, 196 (1998).
[20] T. C. Preston and R. Signorell, J. Chem. Phys. **136**, 094510 (2012).
[21] G. Firanescu, D. Hermsdorf, R. Ueberschaer, and R. Signorell, Phys. Chem. Chem. Phys. **8**, 4149 (2006).
[22] C. F. Bohren and D. R. Huffman, *Absorption and Scattering of Light by Small Particles* (Interscience, New York, 1983).
[23] G. A. Baratta and M. E. Palumbo, J. Opt. Soc. Am. A **15**, 3076 (1998).
[24] U. Kreibig and M. Vollmer, *Optical Properties of Metal Clusters, Materials Science Vol. 25* (Springer, Berlin, 1995).
[25] M. A. Yurkin and A. G. Hoekstra, J. Quant. Spectrosc. Radiat. Transf. **106**, 558 (2007).
[26] Y.-L. Xu, Appl. Opt. **34**, 4573 (1995).
[27] T. C. Preston, G. Firanescu, and R. Signorell, Phys. Chem. Chem. Phys. **12**, 7924 (2010).
[28] G. Cardini, V. Schettino, and M. L. Klein, J. Chem. Phys. **90**, 4441 (1998).
[29] J. A. Barnes, T. E. Gough, and M. Stoer, J. Chem. Phys. **95**, 4840 (1991).
[30] T. E. Gough and T. Wang, Chem. Phys. Lett. **207**, 517 (1993).
[31] R. Disselkamp and G. E. Ewing, J. Chem. Phys. **99**, 2439 (1993).
[32] M. A. Ovchinnikov and C. A. Wight, J. Chem. Phys. **100**, 972 (1994).
[33] T. E. Gough and T. Wang, J. Chem. Phys. **105**, 4899 (1996).
[34] R. Signorell and M. K. Kunzmann, Chem. Phys. Lett. **371**, 260 (2003).
[35] R. Signorell, J. Chem. Phys. **118**, 2707 (2003).
[36] R. Signorell, M. Jetzki, M. Kunzmann, and R. Ueberschaer, J. Phys. Chem. A. **110**, 2890 (2006).
[37] J. P. Devlin, C. A. Yinnon, and V. Buch, Phys. Chem. Chem. Phys. **11**, 7819 (2009).
[38] Ó. F. Sigurbjornsson, G. Firanescu, and R. Signorell, Annu. Rev. Phys. Chem. **60**, 127 (2009).
[39] G. Firanescu, T. C. Preston, C. C. Wang, and R. Signorell, "Vibrational excitons: A molecular model to analyze infrared spectra of aerosols," in *Fundamentals and Applications in Aerosol Spectroscopy*, edited by R. Signorell and J. P. Reid (CRC, Boca Raton, FL, 2011).
[40] T. C. Preston and R. Signorell, Proc. Natl. Acad. Sci. U.S.A. **108**, 5532 (2011).